Author

Xin Wan

Title

Joint seismic and mineral physics modeling of the upper mantle beneath western North America

submitted in partial fulfillment
of the requirements for the degree of
Master of Science in Geology
Department of Geological Sciences
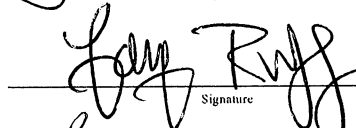The University of Michigan

Accepted by:

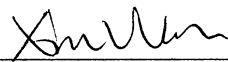|		
Signature	Jeroen Ritsema _Name_	08/08/08 _Date_
Signature	Larry Ruff _Name_	8/12/2008 _Date_
Department Chair	Samuel Mukasa _Name_	8/10/08 _Date_

I hereby grant the University of Michigan, its heirs and assigns, the non-exclusive right to reproduce and distribute single copies of my thesis, in whole or in part, in any format. I represent and warrant to the University of Michigan that the thesis is an original work, does not infringe or violate any rights of others, and that I make these grants as the sole owner of the rights to my thesis. I understand that I will not receive royalties for any reproduction of this thesis.

☒ Permission granted.

☐ Permission granted to copy after: _____
Date

☐ Permission declined.

Author Signature

TITLE:

Joint seismic and mineral physics modeling of the upper mantle

beneath western North America

Abstract

Using 1D seismic velocity profiles we determine whether three complementary sets of seismic observations can be reconciled with simple models for the mantle composition and geotherm. The profiles are founded on self-consistent thermodynamic calculations of phase equilibria, physical properties and seismic velocities. We explore two pyrolitic compositions. Composition EA assumes chemical homogeneity, and composition MM regards the pyrolitic mantle as a mechanical mixture of basalt and harzburgite. Further, we explore more than 1000 geotherms, comprised of linear segments that represent thermal boundary layers and adiabatic segments in the underlying convecting mantle.

Handpicked regional body wave traveltimes, fundamental mode and overtone Rayleigh wave dispersion, and the differential traveltime between converted waves indicate that the upper mantle beneath western North America is relatively hot. The average temperature in the uppermost mantle beneath western North America is at least 1100 K, a value that is consistent with heat flow measurements. The uppermost mantle (<250km) has a relatively steep temperature increase with a gradient of at least 1.75 K/km. In the transition zone, the temperature is about 1900-2000 K. The highest temperatures are resolved for the EA. Temperatures in the MM models are about 100 K lower, indicating the significant influence of mechanical mixing on seismic velocities in the upper mantle.

Keywords: pyrolite, mechanical mixture, Western North America, upper mantle, seismic waves travel times

1. Introduction

With only few geologic sites with exposed mantle rock, the study of earth's inaccessible interior relies almost entirely on remote sensing techniques. Seismology takes an important place in deep earth investigations. By studying the properties of earthquake generated elastic waves, models of Earth's elastic and density structure can be constructed. The very existence of Earth's crust, mantle and core and the primarily layering of the mantle have largely been inferred from seismological data.

Radial symmetric, or 1D, models of Earth's seismic structure (i.e. wave speeds and density) still play a key role in seismology and global geophysics. Beginning with Jeffreys and Bullen (1940), 1D models explain much of the complexity seen in seismograms and indicate that, to first order, Earth's seismic structure changes only as a function of depth. Except in the crust and uppermost mantle, lateral variations in seismic wave speed and density rarely exceed more than a few percent (Romanowicz, 1991).

Traditionally, forward and inverse seismic modeling involves the search for a seismic model that best matches the data without considering whether the resolved models are physically plausible. The character of most seismic models is influenced by the resolving power of the data, choices in parameterization, and artifacts due to theoretical simplifications. Standard, global 1D models such as AK135 (Kennett, 1995) and PREM (Dziewonksi and Anderson, 1981) are non-unique solutions to global data and may have anomalous characteristics (e.g., the 220-km discontinuity in PREM or the density inversion in AK135) that have uncertain geophysical origins.

Model interpretation of seismic profiles or 3D tomographic images based on standard 1D profiles is therefore not straightforward.

Ideally, seismic data are directly modeled using physically meaningful parameters such temperature, composition, or melt content. Recently, Cammarano et al. (2005) have taken such approach on the global scale. They have systematically compared global traveltimes and free-oscillation frequencies to thousand of *"physical reference models"* based on simple mineral physics constraints.

We follow the approach by Cammarano et al. (2005) albeit with a number of important differences. We analyze seismic data on a regional scale and we will employ data types that are strictly sensitive to the upper mantle. We make new measurements using broadband data with established techniques that enable us to quantify measurement uncertainties.

Using theoretical profiles of seismic structure (i.e. physical reference models) based on the thermodynamic method of Stixrude and Lithgow-Bertelloni (2005a,b) and Xu et al. (2008), we will explore whether three complementary sets of seismic observations can be reconciled with 1D profiles. These profiles are based on homogeneous mantle compositions and simple geotherms. For the successful models we will determine the common physical properties.

In sections 2 and 3, we describe the geophysical setting and seismological data. Section 4 provides background on the forward modeling problem and the modeling set up. Results are presented in Section 5 and discussed in Section 6.

2. Study region: the western United States

Western North America is an interesting region with a complex tectonic history (Atwater, 1970) and anomalous geophysical properties. Broad uplift, high heat flow (Pollack et al., 1993), thin lithosphere (Melbourne and Helmberger, 2001) and low seismic velocities (Figure 1) (Grand and Helmberger, 1984a,b) indicate that the temperature in the mantle is anomalously high. Diverse tectonic terrains characterize the region, but the seismic structure in the sublithospheric mantle is within a few percent laterally homogeneous as is evident from the uniformity of teleseismic SS traveltime delays (Grand et al. 1984a,b) and long period surface wave dispersion (Ritsema et al., 2004; Merrer et al., 2007). Previous analyses have suggested elevated temperatures in the region (compared to "normal" continental regions) (Ritsema et al., 2008), not unlike typical values for mid ocean ridges (Herzberg et al., 2007).

Dense regional seismic networks have been operating in the western United States for more than 15 years. Combined, the Berkeley Digital Seismic Network in northern California, operated by UC Berkeley, and TriNet in southern California, operated by the California Institute of Technology and the United States Geological Survey, include more than a 100 stations. Since 2004, the deployment of the Transportable Array, one of the components of the recently launched EarthScope project (www.earthscope.org), have resulted in the operations of more than 400 new stations in the western United States with a stations spacing of about 70 km. The large number of seismic stations (Figure 2) in the western United States and the broadband waveform recording provide us the opportunity to combine array analysis of both

high-frequency body waves and long-period surface wave in our investigations.

3. Seismic data

We analyze three data types with well-established techniques that are applicable to large data volumes. These data types are

1. dispersion of Rayleigh waves,

2. traveltimes of the regional P and S waves, and

3. traveltimes of teleseismic P410s and P660s converted waves.

These seismic phases are sensitive primarily to seismic structure in the upper mantle (< 700 km). Moreover, they provide complementary upper mantle constraints since they have widely different propagations characteristics. Each uniquely constrains absolute velocities, upper mantle and transition zone velocity gradients and the 410-km and 660-km discontinuities depths, structures attributes that depend strongly on the structure of the upper mantle geotherm.

3.1 Rayleigh Wave Dispersion

Rayleigh waves generate the largest amplitude signals in seismograms. Rayleigh waves propagate horizontally through the upper mantle and they are sensitive primarily to the shear velocity. The fundamental mode Rayleigh wave constrains the shallowest regions (0-400 km depth) of the upper mantle. The dispersive character of the Rayleigh waves can be exploited to constrain the variation of shear velocity with depth (Der et al., 1970; Wiggins, 1972). The longest period Rayleigh wave penetrate deepest. Rayleigh wave with periods smaller than 50 s are

affected to great extent by the crust while Rayleigh waves at 200 s period reach a depth of at least 400 km (Figure 3).

Overtone Rayleigh wave are a critical part of our dispersion data set. For the same frequency, overtones penetrate much deeper into the mantle than the fundamental mode and thus help considerably to constrain the seismic structure between 300-500km depth (van Heijst and Woodhouse, 1999; Ritsema et al. 2004).

We use phase velocity dispersion measurements of the fundamental and first overtone Rayleigh wave from 14 shallow and intermediate depth earthquakes in South America and the northwest Pacific. These data have been measured with the U-C diagram technique (Cara, 1978) and modeled previously by (Merrer et al., 2007).

3.2 First Arriving P and S Wave Traveltimes

Regional distance (< 2000km) P and S waves turn within the upper 700 km of the mantle (Figure 4). The derivative of travel time with distance ($\partial T/\partial \Delta$), also called the *ray parameter*, is the inverse of seismic velocity at the turning point of the wave traveling a distance Δ. Measurements of $\partial T/\partial \Delta$ over a broad distance range constrain the vertical shear and P wave velocity gradients.

For 16 earthquakes in Western North America between 2000-2008 with magnitudes larger than 5.5, we measure traveltime curves $T(\Delta)$ of P waves recorded on vertical seismograms and S waves recorded on tangential components seismograms at more than 200 stations (Figure 2). We measure traveltimes from the P and S wave onsets using an interactive computer program. We select highest quality

data after visually inspecting each seismogram. Our data set has twice as many P wave (about 1000 records) measurements than S wave (about 500 records) measurements. Given uncertainties in earthquake location and origin time we can not model absolute traveltimes. Hence we project the traveltimes for all earthquakes onto a single distribution by least-squares minimization.

3.3 Teleseismic P-to-S converted wave traveltimes

P410s and P660s waves are long range P waves that have converted to S waves after crossing the 410-km and 660-km discontinuities beneath the seismic stations (Figure 5). The traveltime difference between P410s and P660s depends entirely on the average shear and P velocity in the transition zone and the depths of the 410-km and 660-km discontinuities. This seismic observable is widely used to constrain the transition zone structure both on a global (Chevrot et al., 1999; Lawrence and Shearer, 2006) and regional scale (Li et al., 2003; Gilbert et al., 2003; Du et al., 2006).

We use radial component seismograms between distances of 56°-88° to measure these traveltimes. The P410s and P660s signals are enhanced by slant stacking. We align all seismograms on the peak of the first arriving P wave and sum the seismograms after applying linear move-out corrections to account for the slightly different slowness of P410s and P660s with respect to P (Vinnik, 1977). On average, we find that, for the western U.S., $T_{P660s}-T_{P410s} = 22.83 +/- 0.3$ s for a P wave slowness of 6s/deg. The 0.3 s uncertainty stems from measurement error and lateral variability in the data.

4. Calculation of 1D seismic velocity structures

4.1 Theory

Predicted values for traveltimes and dispersion are determined by applying the same analytical techniques to synthetic waveforms for theoretical 1D seismic models. The calculation of seismic velocity profiles for two compositions and a range of geotherms are accomplished by a new thermodynamic formulism (Stixrude and Bukowinski, 1993; Stixrude and Lithgow-Bertelloni, 2005a, b; Xu et al., 2008). The procedure involves the calculation of (1) the compositions and proportions of equilibrium phases at certain temperature, pressure and bulk composition, (2) the physical properties of individual phase in the equilibrium compositions, and (3) the elastic properties of the assemblage. Figure 6 illustrates the connection between the theoretical computations and the seismological analysis.

4.2 Model parameterization

Given the computational expense of the theoretical calculations, and the substantial effort to handpick traveltimes in broadband synthetics for each of the 1D profiles, we limit our modeling to relatively few parameters.

4.2.1 Compositions

We explore two compositions for the mantle. Both compositons have the same pyrolitic bulk chemistry but they differ in the manner by which various mantle component are mixed. Pyrolite (Ringwood, 1969), with about 50% olivine, is widely invoked composition for the mantle that is similar to the composition of chondritic

meteorites and it explains, to first order, the seismic velocity structure of the mantle (Bina, 2004)

We will consider the mantle as a mixture of basalt and harzburgite, where the basalt fraction is 15%, consistent with the thickness of the oceanic crust and mid ocean ridge melting depths (Shen and Forsyth, 1995). We determine concentrations of the six most abundant oxides (MgO, FeO, Al_2O_3, SiO_2, CaO, Na_2O) to match the bulk composition of the mantle according to Workman and Hart (2005).

Two end-member models represent two ways harzburgite and basalt can be mixed. The Equilibrium Assemblage (EA) considers full re-equilibration of the basalt and harzburgite into a homogeneous peridotite after the (basaltic) oceanic crust and (harzburgitic) lithosphere re-enter the mantle in subduction zones. The Mechanical Mixture (MM) regards the mantle as a mechanical mixture of basalt and harzburgite that are in chemical disequilibrium. The MM is akin to the "marble-cake" model of (Allègre and Turcotte, 1986) and is motivated by the low rate (10^{-14}– 10^{-16} cm^2/s) of chemical diffusion of mantle in solid state (Allègre and Turcotte, 1986; Farber et al., 1994; Yamazaki, et al., 2000) and long stirring time (250-750 Myr) of the mantle (Kellogg et al., 2002). Although basalt transforms to a denser phase (eclogite) below a depth of 80 km and may settle deep in the mantle (Christensen and Hoffmann, 1994; Brandenburg and Van Keken, 2007), we will ignore the possibility that a basaltic gradient has formed in the mantle (Xie and Tackley, 2004a,b; Nakagawa and Buffett, 2005). Models EA and MM have been discussed in great detail by Xu et al. (2008).

There is not a straightforward way to implement the chemically distinct crust in

our calculations. We therefore substitute the Standard Southern California Velocity Model (Wald et al., 1995; Zhu and Kanamori, 2000) into our theoretical models for the upper 40 km. This simplified model of the crust may affect the accuracy of dispersion of the shortest fundamental mode Rayleigh waves

4.2.3 Geotherms

We consider geotherms that are comprised of two segments. The temperature increases linearly in the uppermost mantle and follows an adiabatic geotherm below it. Three variables define these profiles (Figure 7). T_0 is the temperature at the base of the crust. We explore three values for T_0: 630 K, 1160 K, and 1420 K. The lowest temperature has been suggested as appropriate for the Sierra Nevada region. The highest temperatures represent the range of values estimated for the Basin and Range (Lachenbruch and Sass, 1977).

The geotherm has a kink T_1 at depth z_1. Between the base of the crust and z_1, the temperature increases linearly. Below z_1, the temperature follows an adiabatic geotherm with a potential temperature T. We systematically vary z_1 from a depth of 60 km to 400 km with a 20 km interval. The potential temperature T is varied between 1400 K and 1800 K with a 20 K interval. Therefore, a total of 3x18x21 = 1134 geotherms are explored.

5. Modeling results

For a total of 2268 velocity profiles we calculate Rayleigh wave dispersion using normal mode theory (Gilbert and Dziewonski, 1975), traveltime curves $T(\Delta)$ by

picking onset in broadband synthetic waveforms, and P660s-P410s differential traveltimes from slant stacks of synthetic receiver functions.

For each data set we show the fit to the data as a function of T_1 (along the vertical axis) and Z_1 (along the horizontal axis). Six panels show the fit separately for models MM and EA and three uppermost mantle temperatures of 630 K, 1160 K, and 1420 K. The misfit M is defined by $M = (\sum(D_{syn}-D_{obs})_i^2/E_i^2)/N$, where $(D_{syn}-D_{obs})_i$ is the square difference between observed and predicted value (e.g., the average Raleigh wave phase velocity at a given period i, the average body wave travel $T(\Delta_i)$ at a given distance Δ_i, or the P660-P410s traveltime. E_i is the measurement error in the seismic observable. N is the total number of data points.

5.1 Surface Wave Dispersion

The fit to the fundamental mode and 1st overtone Rayleigh waves are shown in Figure 8 and fits for a selection of profiles are shown in Figure 9. By inspection of the fits, we consider models that produce a misfit M lower than 0.5 as acceptable.

For composition EA these models have values for T_1 between 1540K to 1775K and values for Z_1 that vary between 60km to 400km if we assume a T_0 of 1420K. For the lower T_0 of 1160K, acceptable values for Z_1 range from 70km to 220km.

There is a clear trade-off between Z_1 and T_1. T_1 increases for increasing Z_1. This trade-off is directly linked to integral constraints that dispersion data provide on upper mantle structure. The misfit structure for the EA and the MM are largely the same although a better fit is generally obtained for MM profiles because their shear velocity

gradients are slightly steeper.

The best fitting shear velocity profiles (Figure 10) indicate that the surface wave data requires a negative gradient in $\partial Vs/\partial z$ (i.e. a low velocity zone) just below 100 km depth, and a relatively steep shear velocity gradient between 150 and 400 km depth. The structure of the transition is not well constrained given the relatively large uncertainties of the 1st overtone Rayleigh wave phase velocities.

5.2 First Arriving P and S Wave Traveltimes

Fits to the regional P and S wave traveltimes have nearly identical structure. Hence we show the average misfit of the two data sets (Figure 11). The EA and MM compositions yield similar misfit patterns. From inspection of the fits, we consider profiles that have a misfit lower than 0.4 as acceptable. The profiles with an uppermost mantle temperature T_0 of 630 K produce a low data misfit only if $Z_1 < 200$ Km. Models that fit the data well have a relatively high (> 1600 K) temperature T_1 at a depth z_1 of less than 200 km, indicating that the gradients in the regional traveltimes are best matched when a strong temperature gradient is present in the uppermost mantle. The best fitting shear velocity profiles (Figure 12) and fits to the traveltime curves (Figure 13) indicate, akin to the surface wave data, that best fitting profiles have steep velocity gradients in the upper 400 km of the mantle. The transition zone structure is poorly constrained since the traveltimes of the first-arrival (up to 16 degrees distance) turn well above the 410 km discontinuity.

5.3 P-to-S Conversions

The misfit for the P660-P410s data (Figure 14) indicates that the converted wave traveltimes constrain solely the temperature in the transition zone which is parameterized by T_1. The best fitting profiles for EA have a transition zone temperature that is 100 K higher than for the EA, since transition zone shear velocities are higher in the MM. The range of misfit value is much greater than for the other two data type which indicates that P660s-P410s traveltimes are particularly useful to constrain the temperature in the transition zone. A misfit of less than 1.0 is only achieved for T_1 ranging from 1680K to 1740K for the EA and from 1600K to 1680K for the MM. The best-fitting shear velocity profiles (Figure 15) underscore the tight constraints on the transition zone while shear velocities (and temperature) in the upper mantle is unconstrained.

6. Discussion and Conclusions

Three seismic data sets of body wave traveltimes and Rayleigh wave dispersion provide complementary constraints on the upper mantle shear velocity structure and, temperature gradients. While regional wave traveltimes and Rayleigh wave dispersion suggest steep shear velocity gradients in the upper 400 km of the mantle and a low velocity zone between 100 and 200 km depth (see also Merrer et al. 2007), the P660s-P410s data tightly constrains the shear velocity in the transition zone and the depth of the 410-km and 660-km discontinuities.

By considering the misfit obtained for all three data types, we can determine a population of models that provide adequate fit to the combined data set (Figure 16). Best overall fit is achieved for models in which the uppermost mantle temperature is

1400 K, at the high end of the subcrustal temperature inferred for the Basin and Range. For EA, the temperature at 200 km is equal to 1650-1800 K and subsequently follows the 1700 K adiabat. For the MM, the temperature is about 100 K lower.

Figure 17 shows the velocity profiles of the best fit models along with the shear velocity profiles of model TNA which is derived for tectonic North America (Grand and Helmberger, 1984), PREM, and IASP91. In the upper 200km of the mantle, the shear velocity in MM is higher velocity than in EA and the shear velocity for both models is slightly higher than TNA and significantly lower than PREM and IASP91. Below 200km depth, the shear velocity in both the EA and MM are lower than in TNA and have lower gradients. In the transition zone, the shear velocity in MM is similar to that in TNA. The shear velocity in EA is significantly lower and EA features a wider range of velocity profiles that match the data equally well.

The 410km discontinuities of both EA and MM are deeper than TNA and have a stronger jump. At 660km discontinuity, EA have a stronger jump in velocity than MM.

Overall, the velocity profiles of best fitting models indicate that the geotherm (Figure 18) in the region is relatively hot, consistent with previous studies (Ritsema et al., 2008). Despite a simple parameterization, the best-fitting geotherms share common features. The average temperature in the uppermost mantle beneath western North America is at least 1100K, a value that is consistent with heat flow. The uppermost mantle has a relatively steep temperature increase with a gradient of at least 1.75 K/km. In the transition zone, the temperature is about 1900-2000 K. The

highest temperatures are resolved for the EA. Temperatures in the MM models are about 100 K lower, indicating the significant influence of mechanical mixing on seismic velocities in the upper mantle.

We emphasize the simplicity of the models explored and we readily acknowledge that important seismic data types have not been considered. We have ignored compositional and thermal heterogeneity, the presence of partial melt (Hammond and Humphreys, JGR 2000), hydrous phases (Bercovici and Karato, Nature, 2003), and other traces element. Furthermore, we have ignored the effects of anisotropy that can be constrained from combined Love and Rayleigh wave analysis (Gaherty, 2001) and SKS splitting (Silver and Holt, 2002) and amplitude of P410s and P660s (Lawrence and Shearer, 2006) that may further constrain the velocity jumps in the transition zone.

The modeling exercise presented here offers a recipe to constrain the first order features of seismological models that can readily be related to known physical parameters and that could serve a physical reference model for subsequent detailed modeling and tomographic imaging.

7. References

Allegre, C. J. and Turcotte, D. L., Implications of a two-component marble-cake mantle, Nature, 323, 123-127, 1986.

Atwater T., Implications of plate tectonics for the Cenozoic tectonic evolution of western North America, Bull. Geol. Soc. Amer., 81, 3513-3536, 1970.

Bercovici, D. and S. i. Karato, Whole mantle convection and the transition-zone water filter, Nature 425, 39-44, 2003.

Bina, C.R., Seismological Constraints upon Mantle Composition. In: Treatise on Geochemistry. Holland, H.D. and Turrekian, K.K. (Editors), Elsevier, Amsterdam, The Netherlands. 2: 39-59, 2004.

Brandenburg, J. P., Van Keken, P. E., Deep storage of oceanic crust in a vigorously convecting mantle. J. Geophys. Res., 112, B06403, 2007.

Cammarano, F., A. Deuss, S. Goes, and D. Giardini, One-dimensional physical reference models for the upper mantle and transition zone: Combining seismic and mineral physics constraints, J. Geophys. Res., 110 (b1), 2005, p.B01306, doi:10.1029/2004JB003272, 2005.

Cara M., Regional variations of higher Rayleigh-mode phase velocities: a spatial-filtering method, Geophysical Journal of the Royal Astronomical Society, 54, 439-460, 1978.

Chevrot, S., L. Vinnik, and J.-P. Montagner, Global-scale analysis of the mantle Pds phases, J. Geophys. Res., 104(B9), 20203-20219, 1999.

Christensen Ulrich R. and Albrecht W. Hofmann, Segregation of subducted oceanic crust in the convecting mantle, J. Geophys. Res., 99, B10, 19,867–19,884, 1994.

Der, Z., R. Masse, and M. Landisman, Effect of observational errors on the resolution of surface waves at intermediate distance, J. Geophys. Res., 75, 3399, 1970.

Du Z., L.P. Vinnik, G. R. Foulger, Evidence from P-to-S mantle converted waves for a flat "660-km" discontinuity beneath Iceland, Earth and Planetary Science Letters 241, 271– 280, 2006.

Dziewonksi, A.M., Anderson, D.L., Preliminary reference Earth model, Phys. Earth Planet. Inter. 25, 297–356, 1981.

Farber D.L., Willams Q., Ryerson F.J., Diffusion in Mg2SiO4 polymorphs and chemical heterogeneity in the mantle transition zone, Nature 371 (6499): 693-695, 1994.

Gaherty James B., Seismic Evidence for Hotspot-Induced Buoyant Flow Beneath the Reykjanes Ridge, Vol. 293. no. 5535, pp. 1645 – 1647, DOI: 10.1126/science.1061565, Science, 2001:

Gilbert, F. and A.M. Dziewonski, An application of normal mode theory to the retrieval of structural parameters and source mechanisms from seismic spectra, Phil. Trans. Roy. Soc. London A278, 187-269, 1975.

Gilbert, H. J., Sheehan, A. F., Dueker, K. G. & Molnar, P. Receiver functions in the western United States, with implications for upper mantle structure and dynamics. J. Geophys. Res. 109(B5), doi:10.1029/2001JB001194, 2003.

Grand, S. P., Helmberger, Donald V., Upper mantle shear structure beneath the northwest Atlantic Ocean, J. Geophys. Res., 89, B13, 11465-11475, 1984a.

Grand, Stephen P.; Helmberger, Donald V., Upper mantle shear structure of North America, Geophys. J. R. astr. Soc. 76, 399-438, 1984b.

van Heijst, Hendrik Jan; Woodhouse, John, Global high-resolution phase velocity distributions of overtone and fundamental-mode surface waves determined by mode branch stripping, Geophysical Journal International, Volume 137, Issue 3, pp. 601-620, 1999

Herzberg, C., P., D. Asimow, N. Arndt, Y. Niu, C. M. Lesher, J. G. Fitton, M. J. Cheadle and

A. D. Saunders, Temperatures in ambient mantle and plumes: Constraints from basalts, picrites, and komatiites, Geochem. Geophys. Geosyst. 8, 2007.

Irifune,T., Phase transformation in the earth's mantle and subducting slabs: Implications for their compositions, seismic velocity and density structures and dynamics. Island Arc 2, 55-71, 1993.

Ita, J. J., and Stixrude, L., Petrology, elasticity and composition of the transition zone. J. Geophys. Res. 97, 6849-6866. 1992.

Jeffreys H. and K.E. Bullen, Seismological tables, British Association for the Advancement of Science, London, 1940.

Kellogg, J.B., Jacobsen, S.B. and Connell, R.J., Modeling the distribution of isotopic ratios in geochemical reservoirs, Earth Planet. Sci. Lett., 204, 183-202, 2002.

Kennett B. L. N., and E. R. Engdahl, Traveltimes for global earthquake location and phase identification, Geophys. J. Int., 105, 429-465, 1991.

Kennett B.L.N., Engdahl E.R. and Buland R., Constraints on seismic velocities in the Earth from travel times, Geophys J Int, 122, 108-124, 1995.

Lachenbruch, A. H. and Sass, J. H., Heat flow and the thermal regime of the crust, in J. G. Heacock., The earth's crust, its Nature and physical properties, American Geophysical Union, Washington, D. C., 625-675, 1977.

Lawrence, J.F., and P.M. Shearer, A global study of transition zone thickness using receiver functions, J. Geophys. Res., 111, dio:10.1029/2005JB003973, 2006.

Li X., R. Kind, X. Yuan, S. V. Sobolev, and W. Hanka, D. S. Ramesh, Y. Gu and A. M. Dziewonski Seismic observation of narrow plumes in the oceanic upper mantle, Geophys. Res. Lett., 30, 6, 1334, doi:10.1029/2002GL015411, 2003.

Melbourne, T. and D. V. Helmberger, Mantle Control of Plate Boundary deformation with P and S Waves, Geophys. Res. Lett., 28, No. 20, 4003-4006, 2001.

Merrer S., Cara M., Rivera L., Ritsema J., Upper mantle structure beneath continents: New constraints from multi-mode Rayleigh wave data in western North America and southern Africa, Geophys. Res. Lett., 34, L06309, doi:10.1029/2006GL028939, 2007

Nakagawa, T., and B. A. Buffett, Mass transport mechanism between the upper and lower mantle in numerical simulations of thermo-chemical mantle convection with multi-component phase changes, Earth Planet Sci. Lett., 230, 11-27, 2005.

Pollack H. N., Suzanne J. Hurter and Jeffrey R. Johnson, Heat Flow from the Earth's Interior: Analysis of the Global Data Set, Rev. of Geophys., 31, 3, 267–280, 1993.

Ringwood, A. E. 1969 Composition and evolution of the upper mantle. In The Earth's crust and upper mantle (ed. P. J. Hart), pp. 1-17. Am. Geophys. Mongr. Ser. 13, Washington, D. C., 1969

J. Ritsema, and R. M. Allen, The elusive mantle plume, Earth and Planetary Science Letters, 207, 1-12, 2003.

Ritsema J., Heijst H. J., and Woodhouse J. H., Global transition zone tomography, J. Geophys. Res. 109, B02302, doi:10.1029/2003JB002610, 2004

Ritsema, J., The modeling of Ps converted waves with physical references earth models, AGU abstract, 2006

Ritsema et al., Estimate mantle temperature variation from seismic and mineral physics constraints, Geology, in review, 2008

Romanowicz, B., Seismic tomography of the earth's mantle, Ann. Rev. of Earth and Planet. Sci., 19, 77-99, 1991.

Shen, Y. and D.W. Forsyth, Geochemical constraints on initial and final depths of melting

beneath mid-ocean ridges, J. Geophys. Res., 100, 2211-2237, 1995.

Silver P. G. and W. E. Holt, The Mantle Flow Field Beneath Western North America, Vol. 295. no. 5557, pp. 1054 – 1057, DOI: 10.1126/science.1066878, Science, 2002.

Stixrude, L. and C. Lithgow-Bertelloni, Mineralogy and elasticity of the oceanic upper mantle: Origin of the low velocity zone, Journal of Geophysical Research, 110, B03204, doi: 10.1029/2004JB002965, 2005a.

Stixrude, L. and M. S. T. Bukowinski, Thermodynamic analysis of the system MgO-FeO-SiO2 at high pressure and the structure of the lowermost mantle, in Evolution of the Earth and Planets, Geophysical Monograph 74, edited by E. Takahashi, R. Jeanloz, and D. Rubie, International Union of Geodesy and Geophysics and American Geophysical Union, Washington, D. C., pp. 131-141, 1993.

Stixrude, L. and C. Lithgow-Bertelloni, Thermodynamics of mantle minerals: 1. Physical properties, Geophysical Journal International, 162, 610-632, 2005b.

Vinnik, L. P., Detection of waves converted from P to SV in the mantle, Physics of the Earth and Planetary Interiors, Volume 15, Issue 1, p. 39-45., 10.1016/0031-9201(77)90008-5, 1977

Wald, L. A., L. K. Hutton, and D. D. Given, The Southern California Seismic Network bulletin: 1990 - 1993 Summary, Seismol. Res. Lett. 66, 9 – 19, 1995.

Weidner, D.J, A mineral physics test of a pyrolite mantle. Geophys. Res. Lett. 12, 417-420, 1985.

Wiggins, R.A., The general linear inverse problem: implication of surface waves and free oscillations for earth structure, Rev. Geophys. Space Phys., 10, 251, 1972.

Workman, R.K. and Hart, S.R., Major and trace element composition of the depleted MORB mantle (DMM). Earth and Planetary Science Letters 231: 53-72, 2005.

Xie, S. and P. J. Tackley, Evolution of U-Pb and Sm-Nd systems in numerical models of mantle convection. Journal of Geophysical Research 109, 2004a.

Xie S. and P.J. Tackley, Evolution of helium and argon isotopes in a convecting mantle, Phys. Earth Planet. Inter. 146, 417–439, 2004b.

Xu W, Lithgow-Bertelloni C. Stixrude L. and Ritsema J., The effect of bulk composition on seismic structure, in submit, 2008.

Yamazaki D, Kato T, Yurimoto H, et al., Silicon self-diffusion in MgSiO3 perovskite at 25 GPa, Phys. Earth Plant. Int. 119: 299-309, 2000.

Zhu and Kanamori, Moho depth variation in southern California from teleseismic receiver functions, Journal of Geophysical Research, Volume 105, Issue B2, p. 2969-2980, 2000.
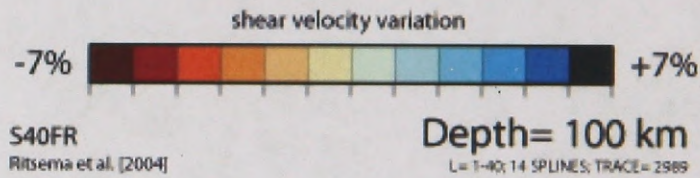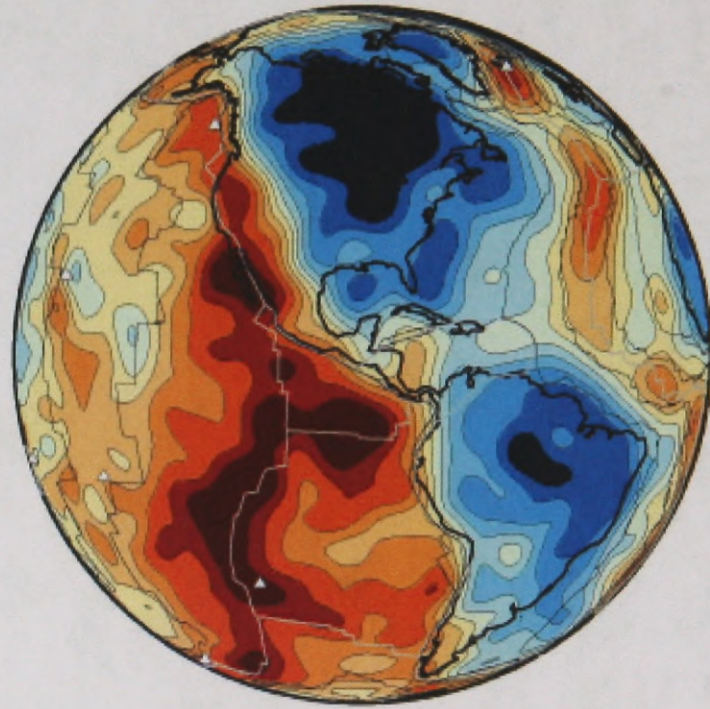
Figure 1. Map of shear velocity variation at a depth of 100 km according to model S20RTS (Ritsema et al., 2004). The shear velocity in regions shaded red (blue) are up to 7% lower (higher) than the average shear velocity at 100 km depth. White triangles are hotspot location from the compilation of Ritsema and Allen (2003). Note that at this large scale the shear velocities beneath the western United States and the East Pacific Rise region are similarly low.
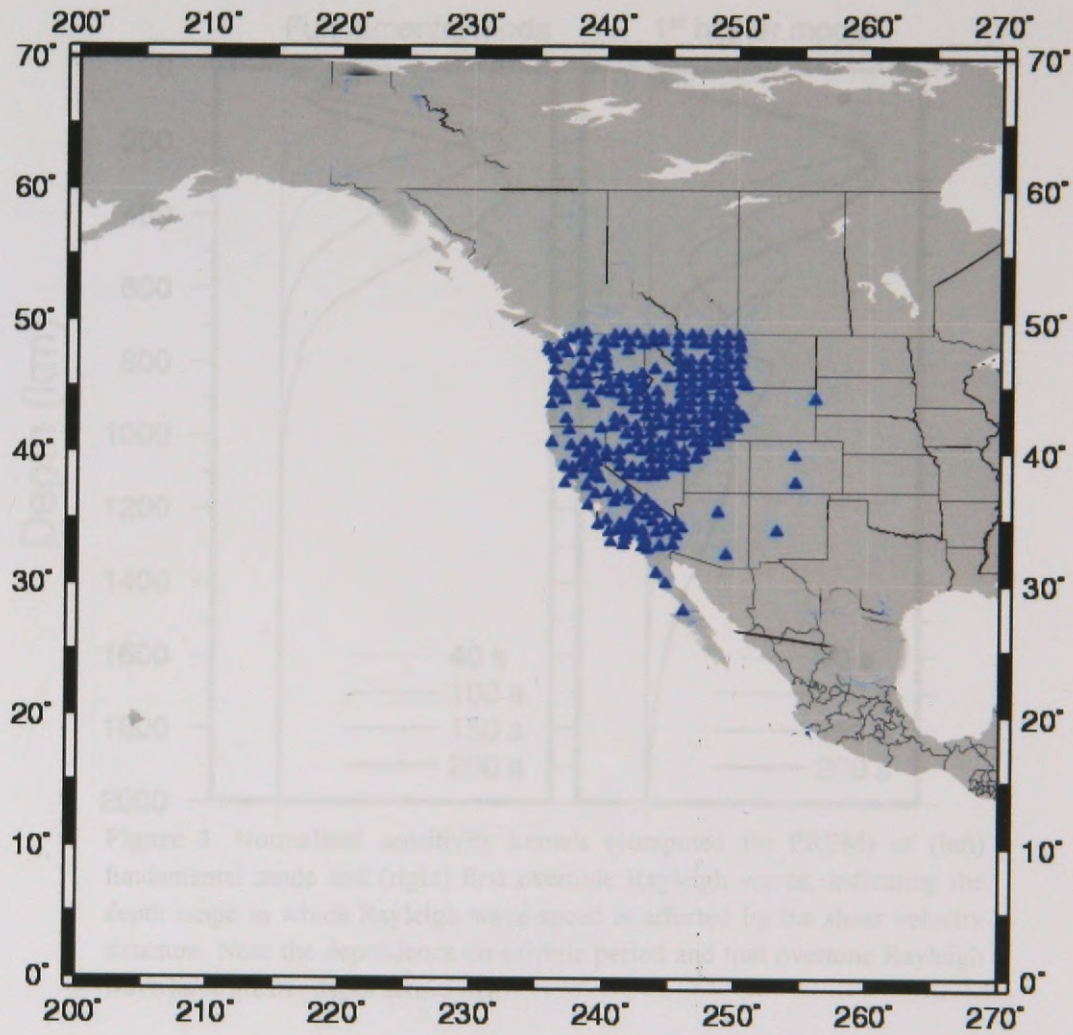
Figure 2. Locations of broadband digital stations in western North America from the Berkeley Digital Seismic Network, TriNET, NARS-Baja, the Transportable Array and the United State National Seismic Network.
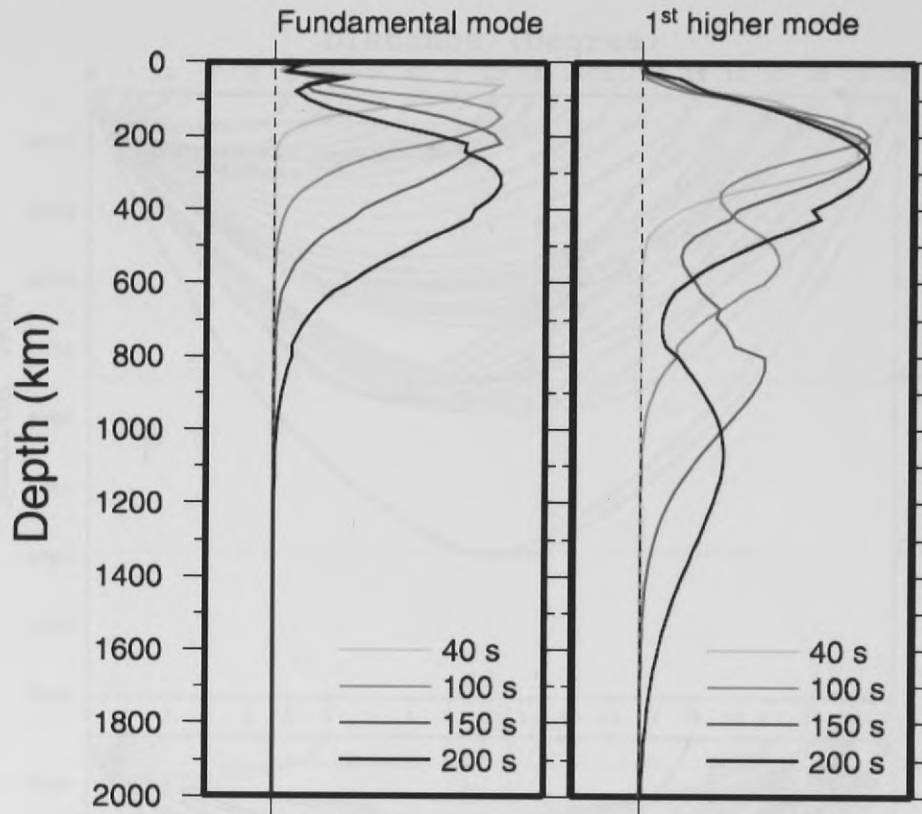
Figure 3. Normalised sensitivity kernels (computed for PREM) of (left) fundamental mode and (right) first overtone Rayleigh waves, indicating the depth range in which Rayleigh wave speed is affected by the shear velocity structure. Note the dependence on seismic period and that overtone Rayleigh wave have greater depth sensitivity.
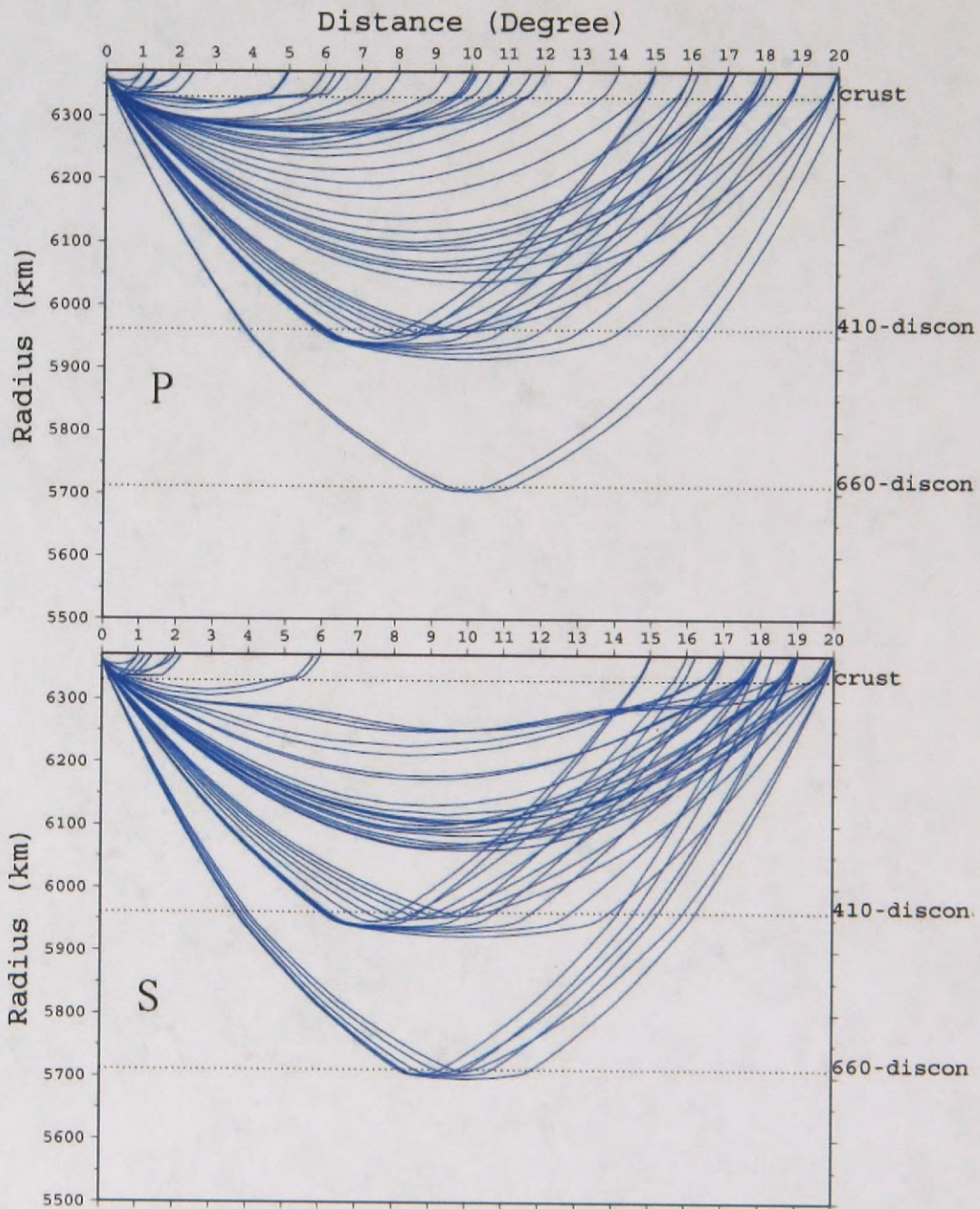
Figure 4. Geometrical ray paths of (top) P and (bottom) S waves propagating at regional distances up to 20°. Note the triplications, indicating that three P or S waves arrivals can be recorded at a single distance due to the discontinuous velocity changes at the 410-km and 660-km phase transitions.
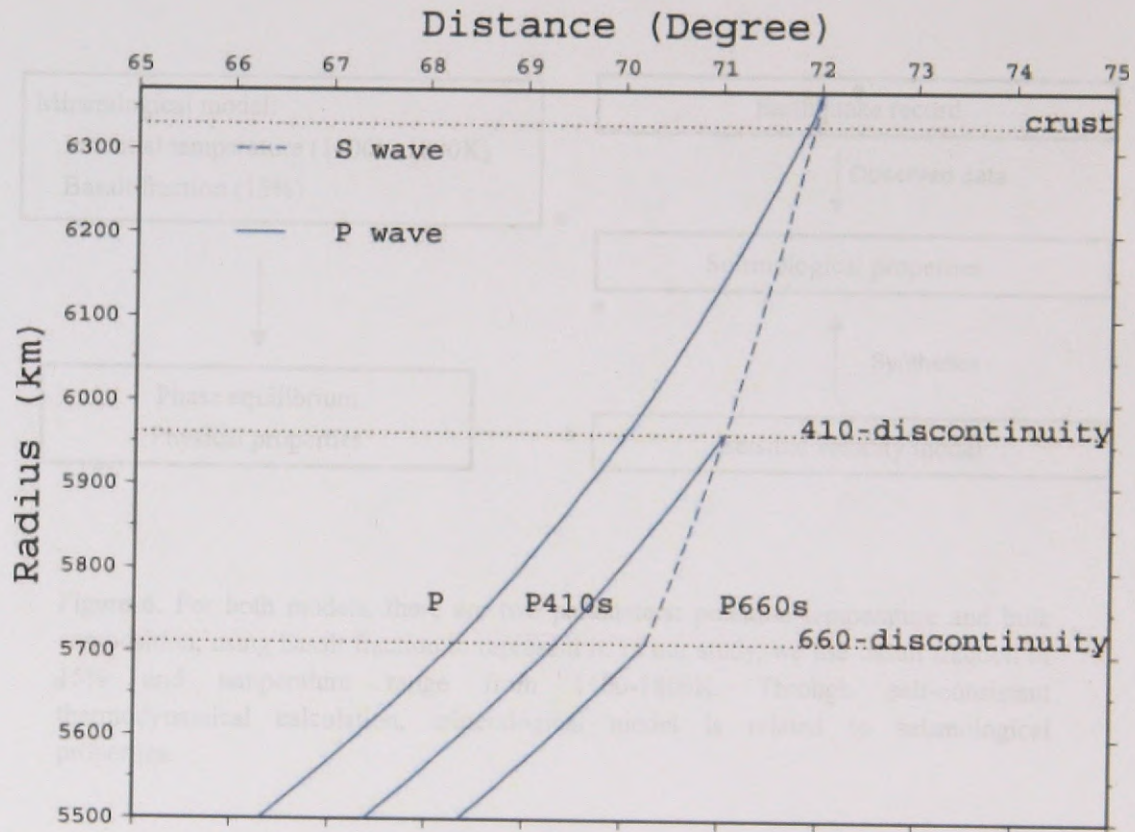
Figure 5. Geometrical ray paths of the P, P410s and P660s waves. P wave segments are indicated by solid lines, S wave segments are indicated by dashed lines. Note the similarity of P410s and P660s waves except in the transition zone where P410s propagates as a P wave and P660s as an S wave.
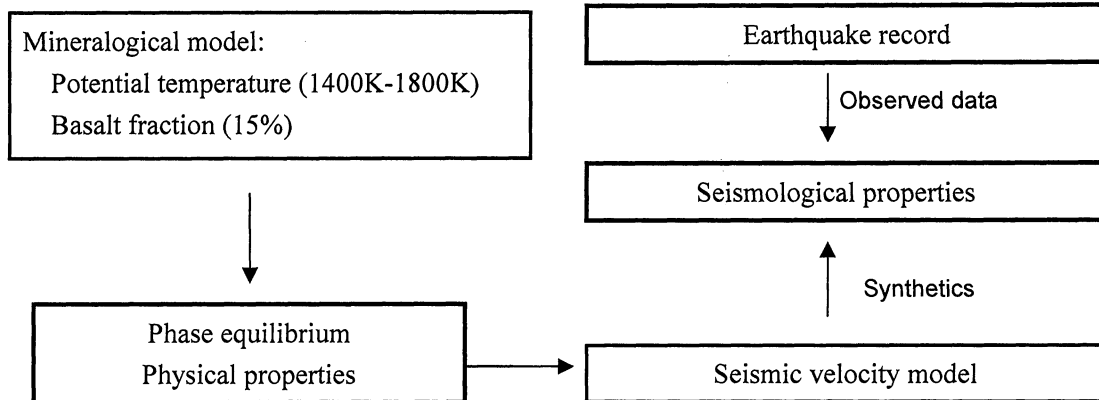
Figure 6. For both models, there are two parameters: potential temperature and bulk composition, using basalt fraction to represent it. In our study, we use basalt fraction of 15% and temperature range from 1400-1800K. Through self-consistent thermodynamical calculation, mineralogical model is related to seismological properties.
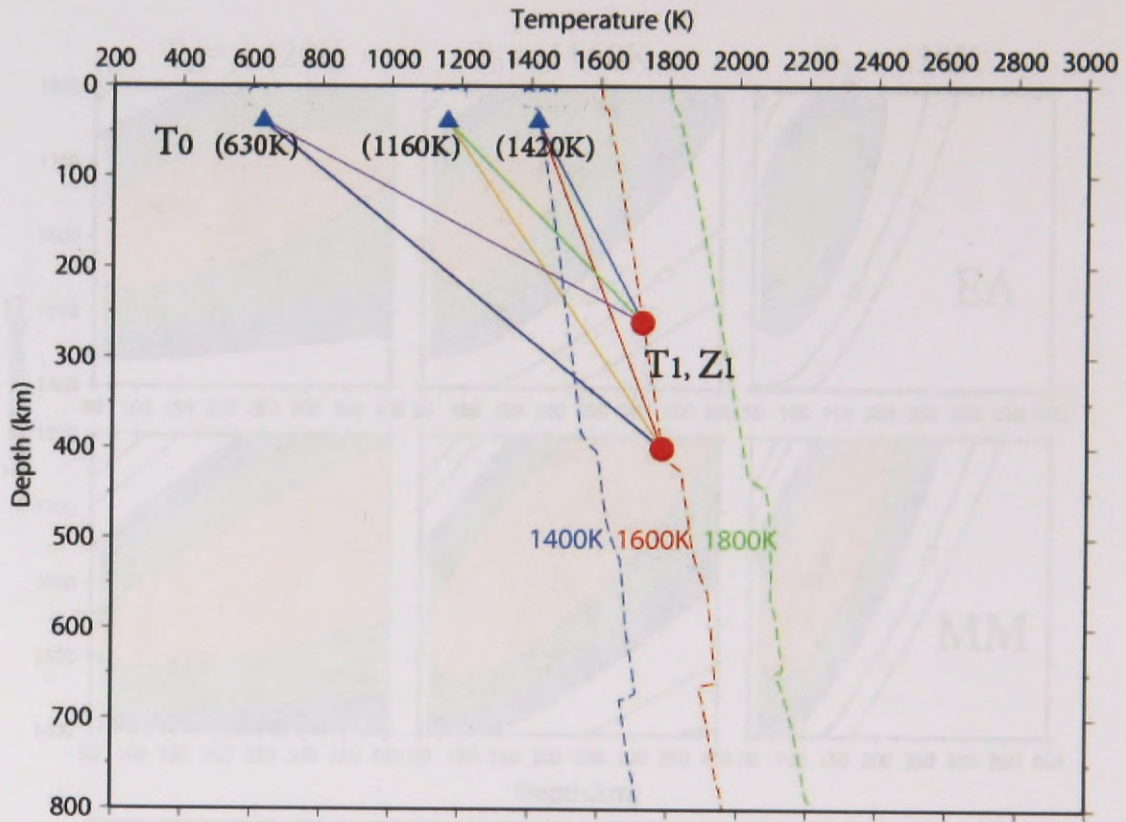
Figure 7. Example geotherms, illustrating how three parameters used to parameterize the shape of the geotherms. T_0 is the temperature at the base of the crust (z_0). The temperature increases linearly between z_0 and z_1. Below z_1, the temperature follows a mantle adiabat with a potential temperature of T_1. Shown are adiabats for potential temperatures of (blue) 1400 K, (red) 1600 K and (green) 1800 K.
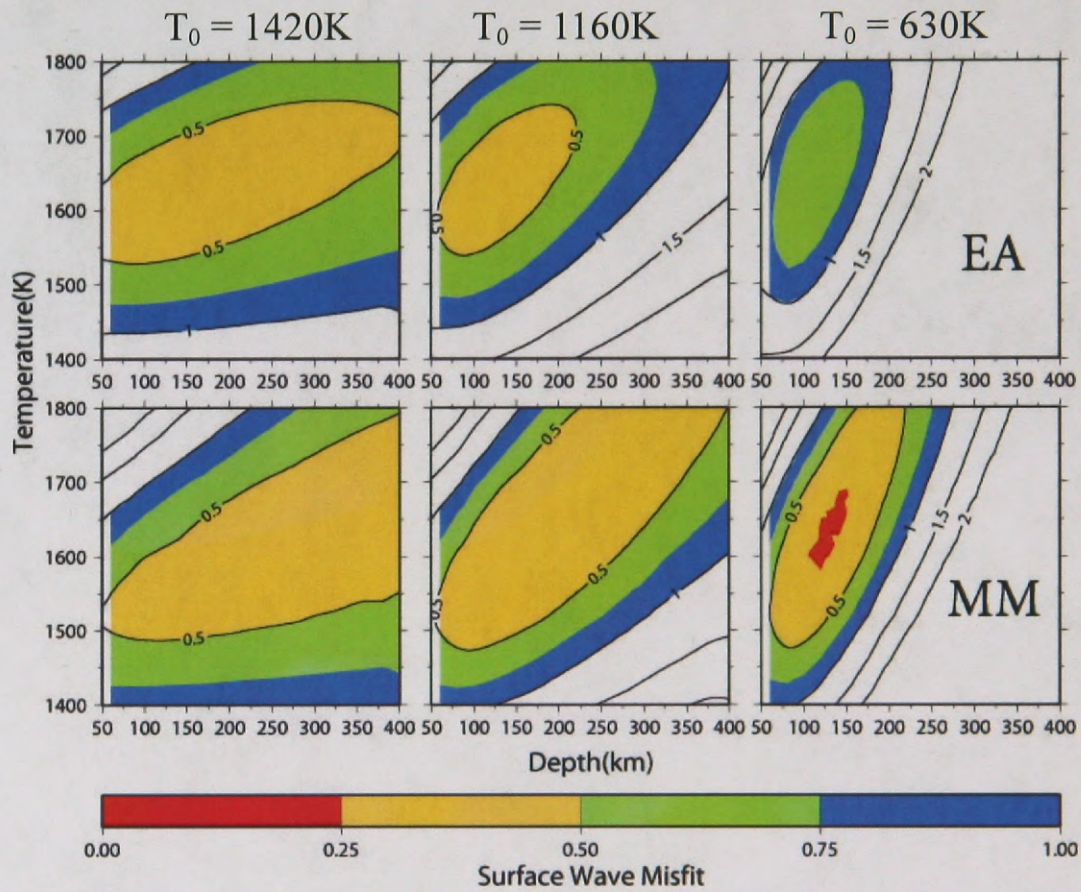
Figure 8. Misfit between the prediected and observed Rayleigh wave dispersion as a function (vertical axis) T1 and (horizontal axis) z1. The six panels show misfit for temperature T0 of (right) 630 K, (middle) 1160 K, and (left) 1420 K.EA and for the (top) EA and (bottom) MM compositions.
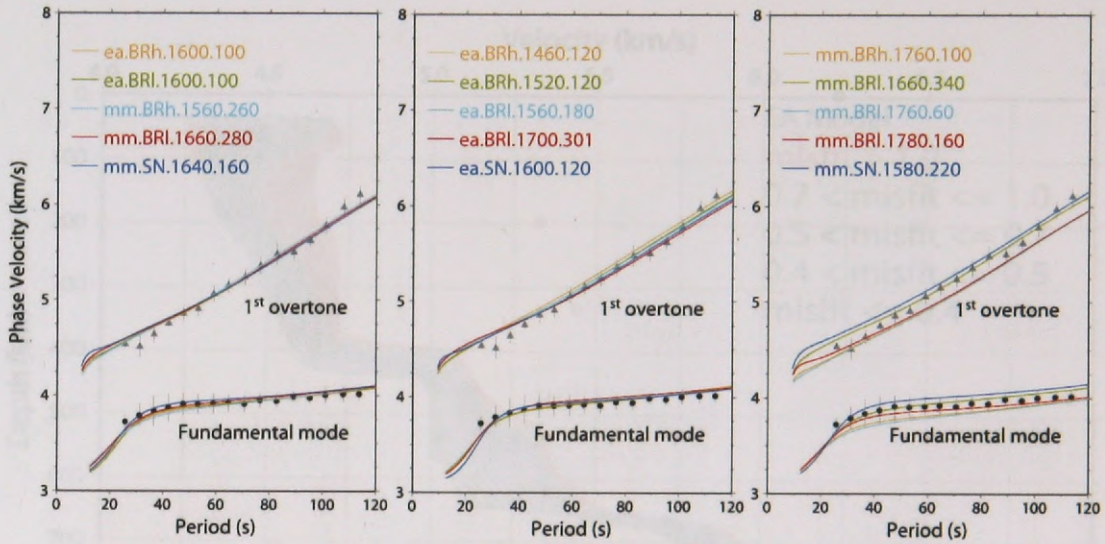
Figure 9. Comparison of (black circles) observed and (colored lines) predicted Rayleigh wave phase velocities for a selection of models. (left) model yielding a misfit M<0.5, (middle) models yielding a misfit 0.5<M<0.7, and (right) models yielding a misfit M>1.0
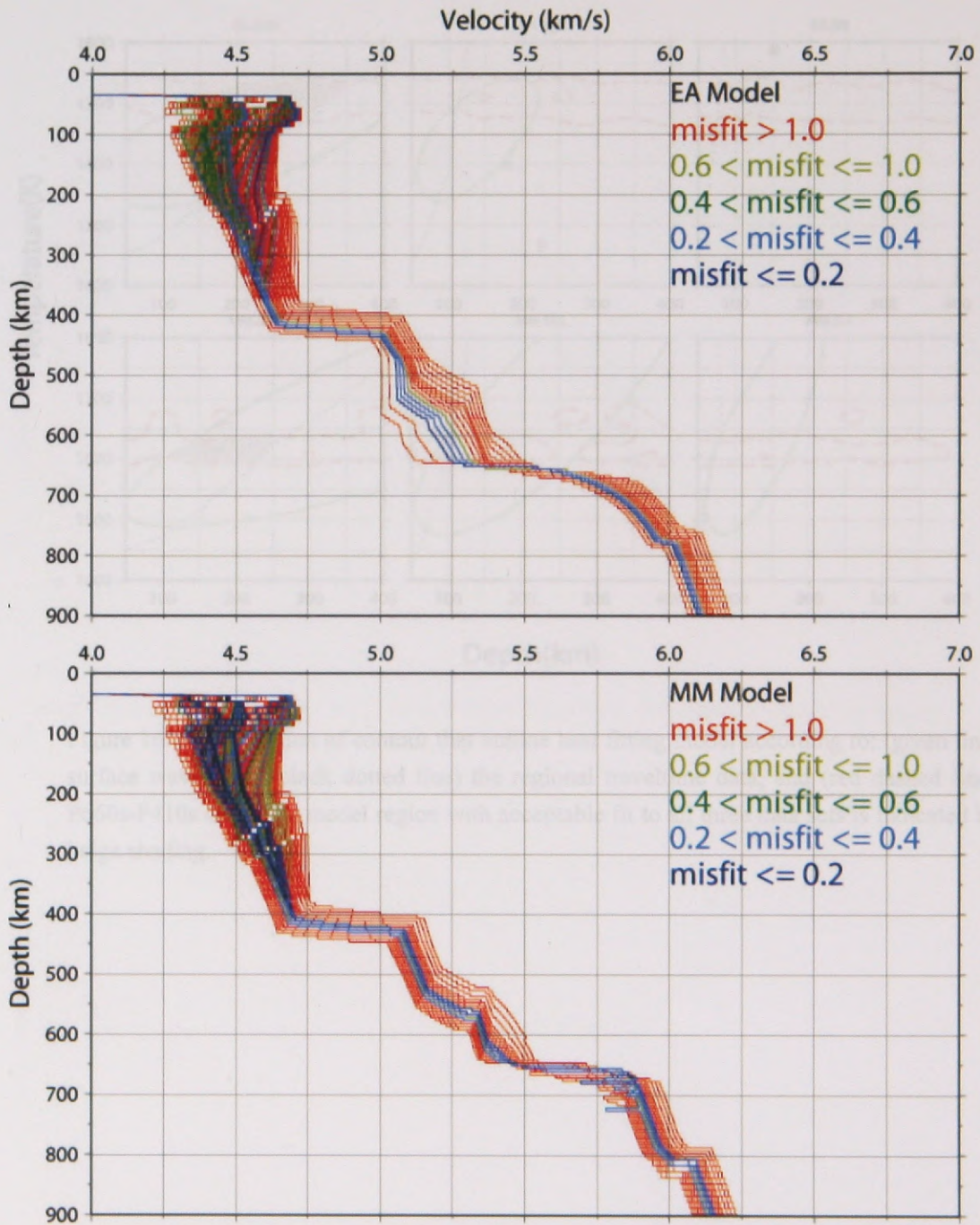
28

Figure 10. Shear wave velocity profiles colour-coded according to how well they explain surface wave dispersion data: The profiles produce misfit values of: (dark blue) M< 0.4, (light blue) 0.4<M<0.5 (dark green) 0.5<M<0.7 (light green) 0.7<M<1.0, and (red) M>1.0.
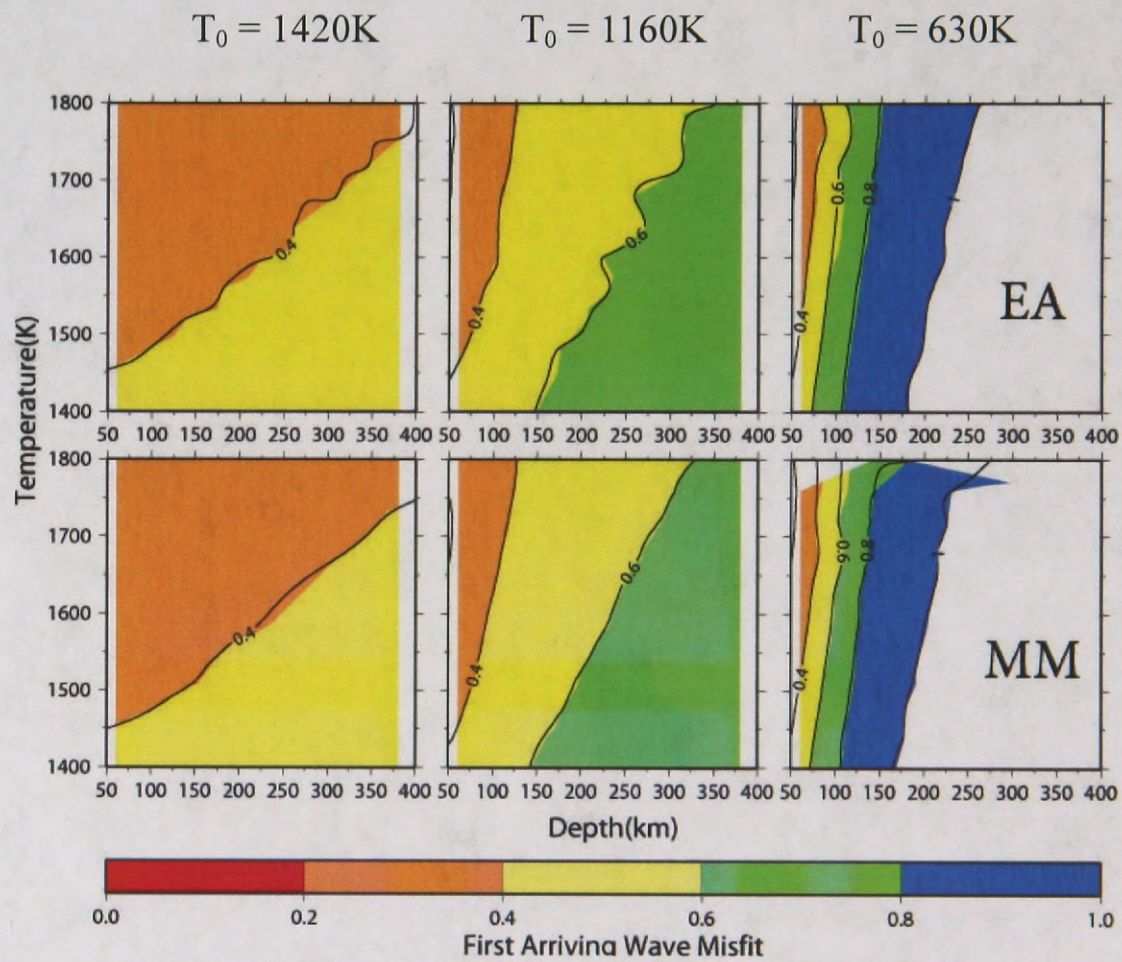
Figure 11. Misfit between the predicted and observed regional travel times. See Figure 8 for further detail.
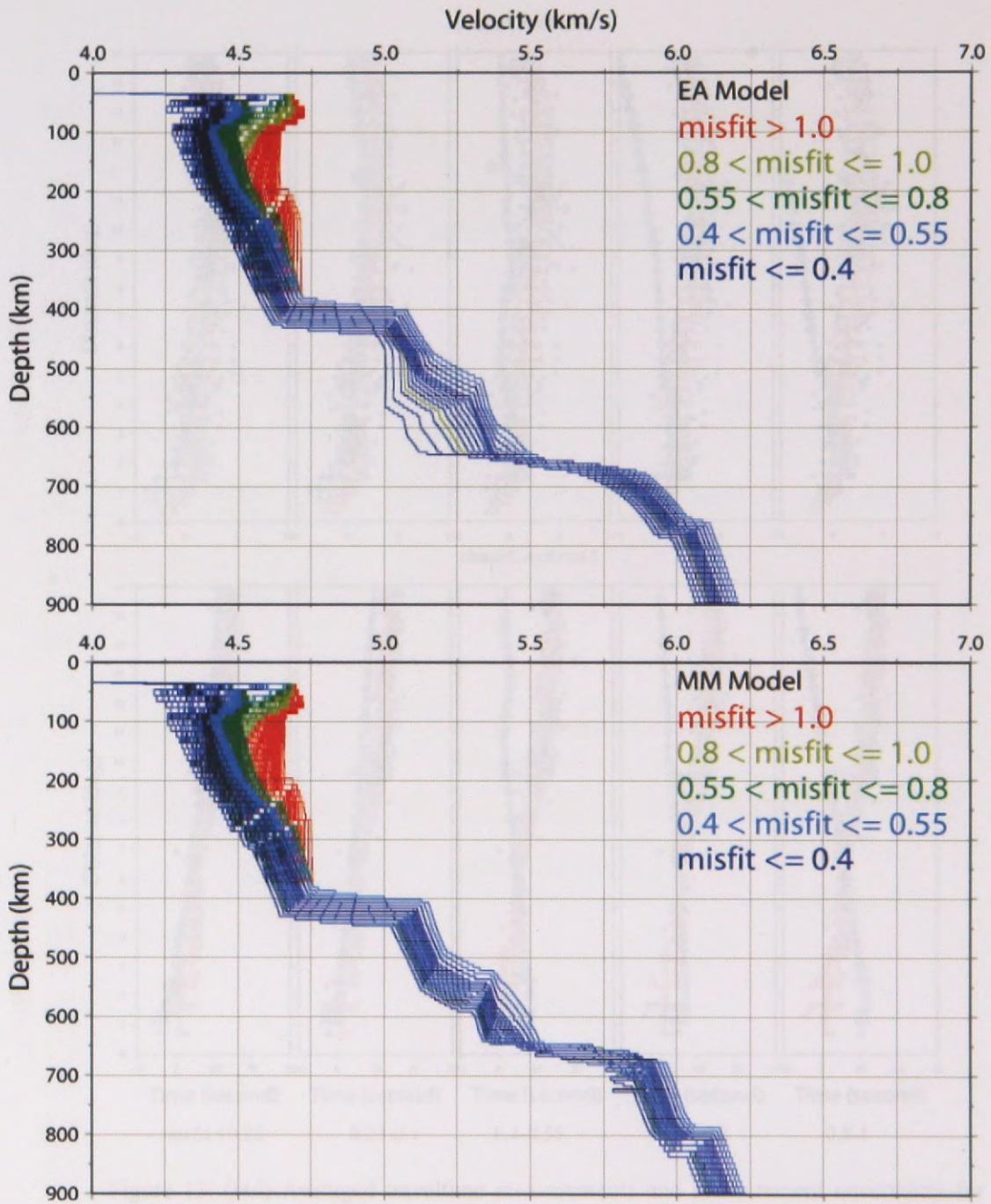
Figure 12. Shear wave velocity profiles colour-coded according to how well they explain regional traveltime data data: The profiles produce misfit values of: (dark blue) M< 0.4, (light blue) 0.4<M<0.55 (dark green) 0.55<M<0.8 (light green) 0.8<M<1.0, and (red) M>1.0.
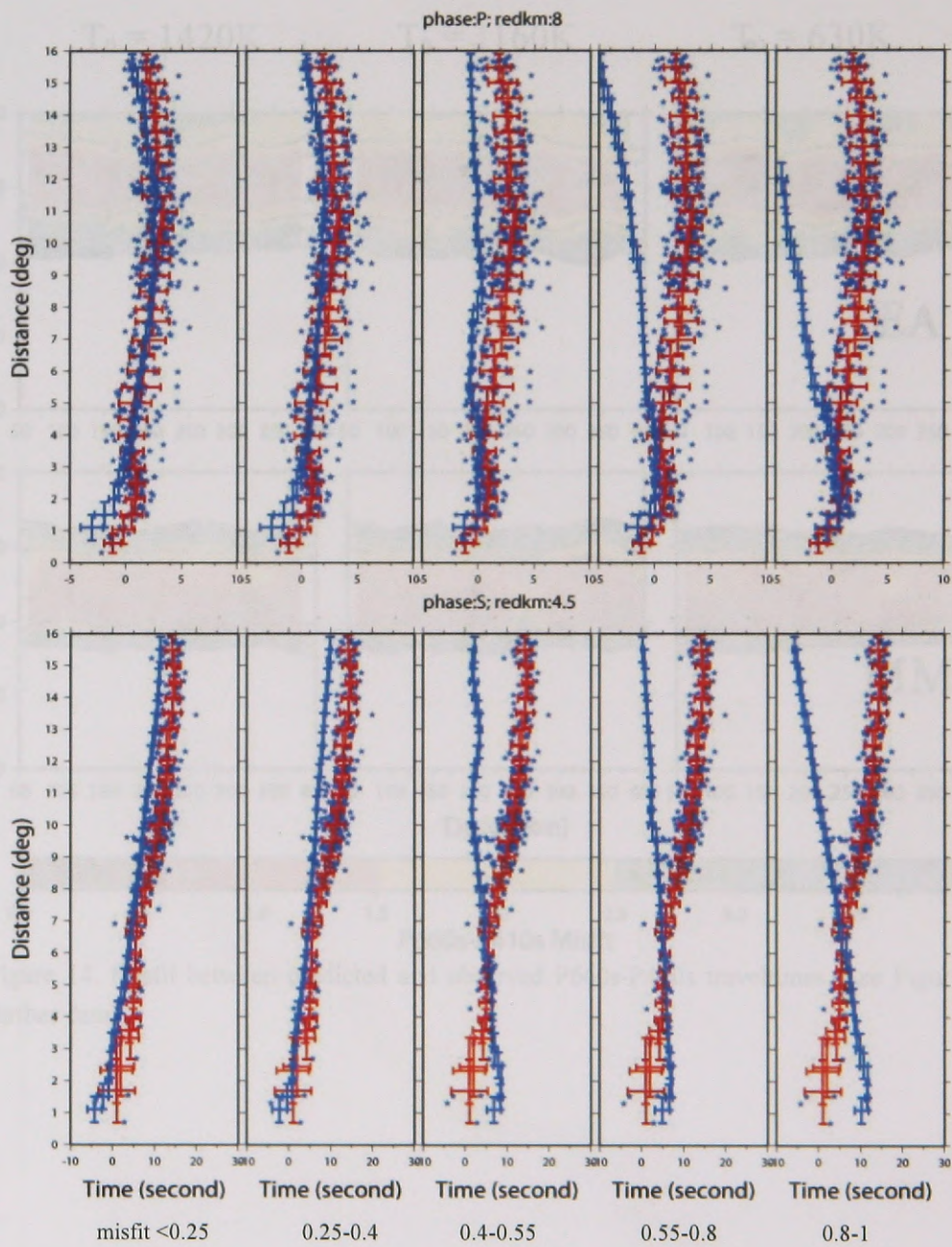
Figure 13. (red) Averaged traveltime measurements and measurement uncertainty for (top) P and (bootom) S waves and (blue) predicted values for selected models that yield a misfit of (from left to right) M<0.25, 0.25<M<0.4, 0.4<M<0.55,0.55<M<0.8, and 0.8<M<1.0 for slope of traveltime curve.
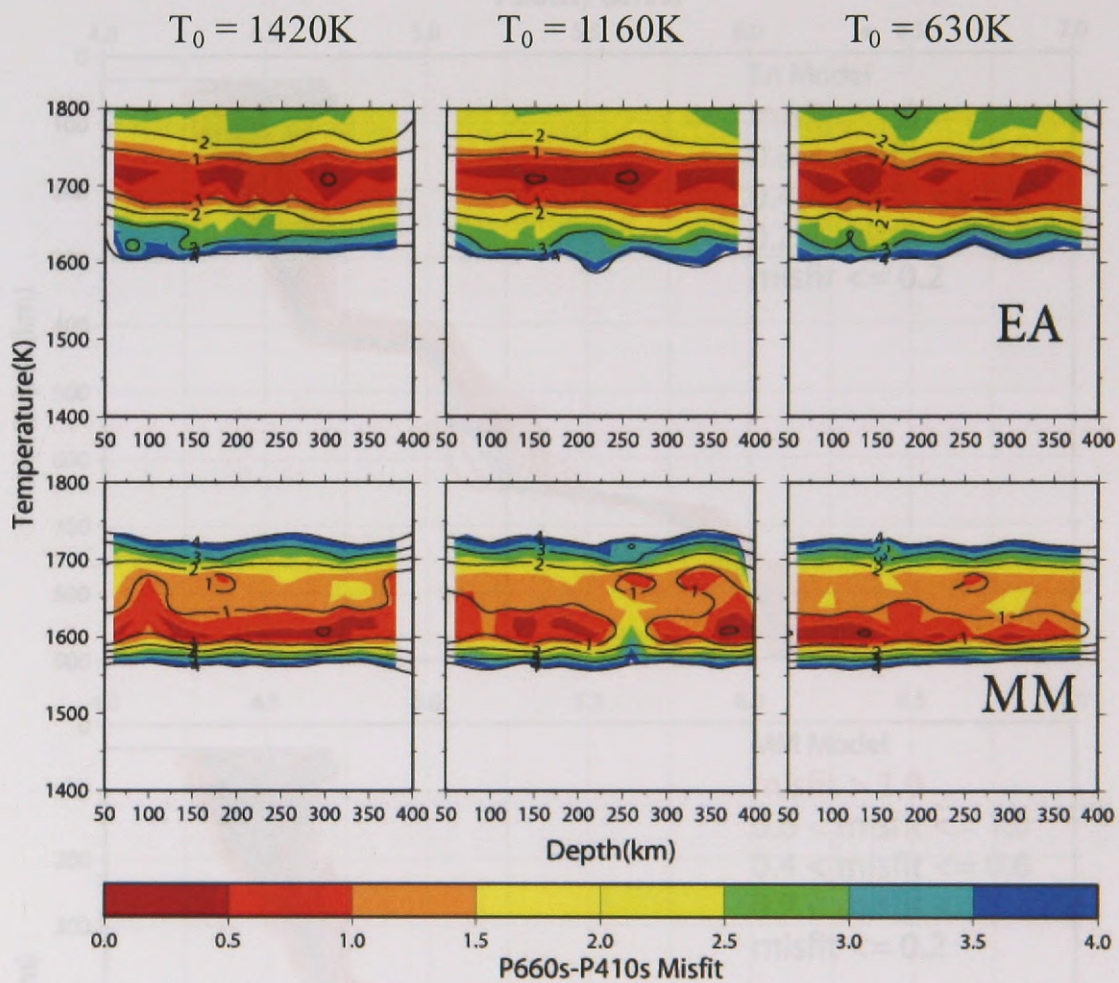
Figure 14. Misfit between predicted and observed P660s-P410s traveltimes. See Figure 8 for further detail.

Figure 15. Shear wave velocity profiles colour-coded according to how well they explain P660s-P410s data: The profiles produce misfit values of: (dark blue) M< 0.2, (light blue) 0.2<M<0.4 (dark green) 0.4<M<0.6 (light green) 0.6<M<1.0, and (red) M>1.0.

Figure 16. Superposition of contour that outline best fitting model according to: (green line) the surface wave data, (black dotted line) the regional traveltime data, and (red dashed line) the P660s-P410s data. The model region with acceptable fit to all three data sets is indicated by the beige shading.
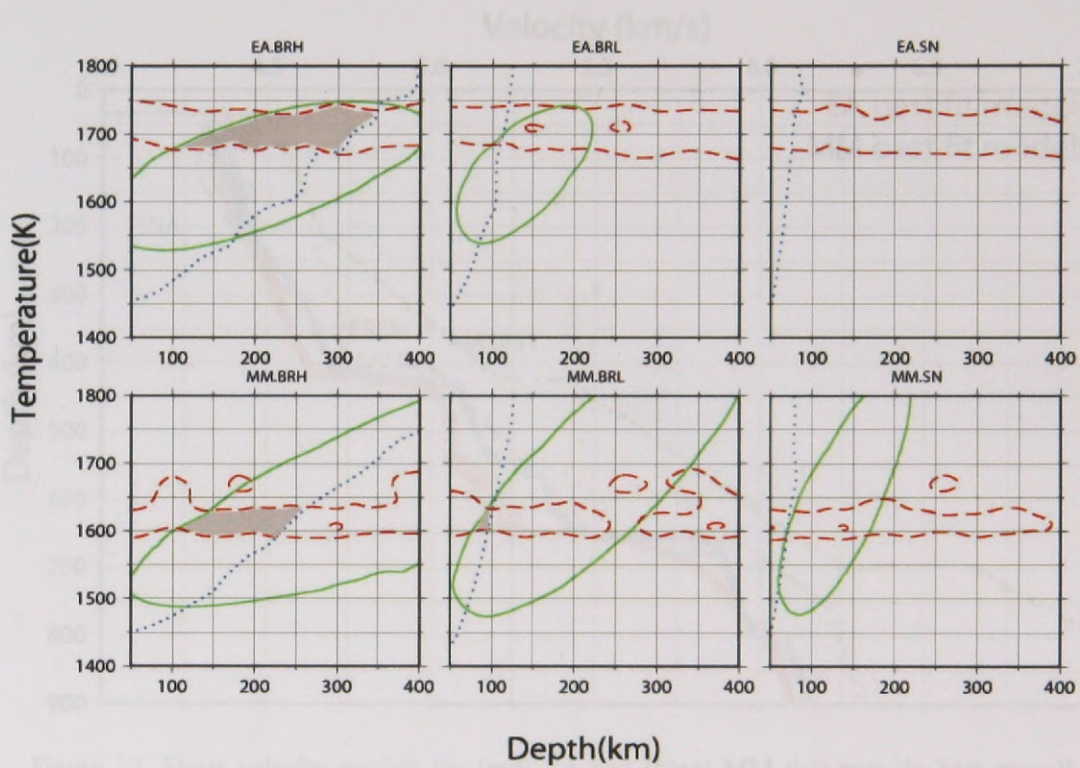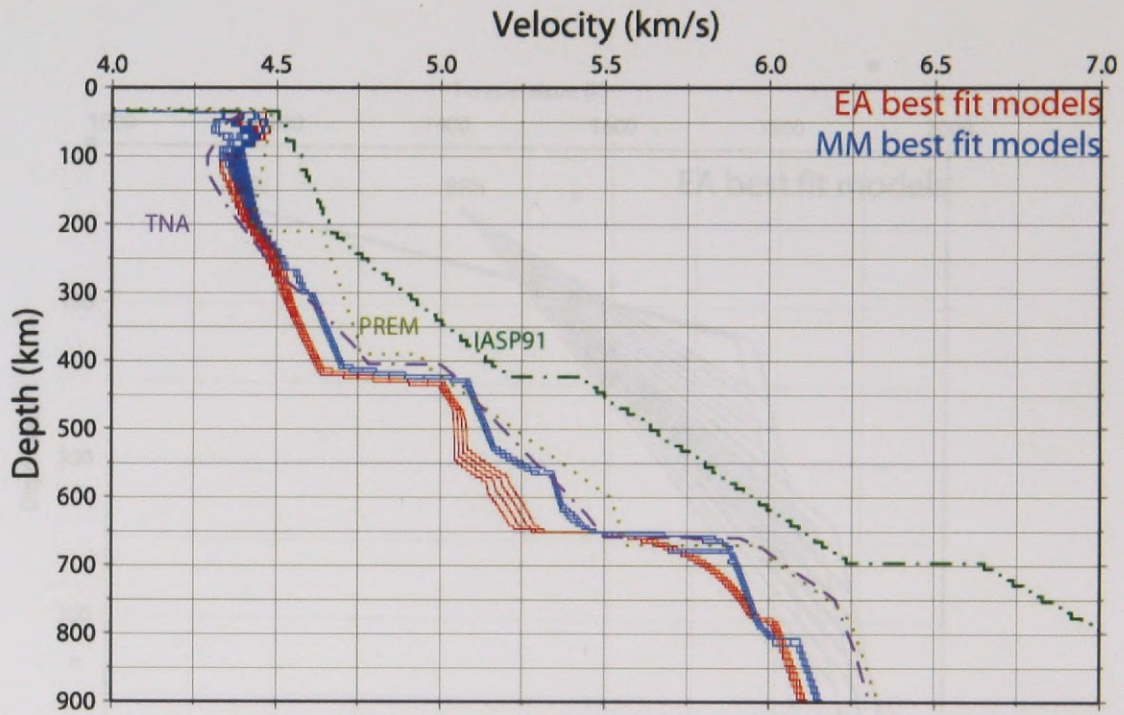
Figure 17. Shear velocity models for (red) EA and (blue) MM that provide best overall match to the regional travel times, surface wave dispersion, and P660s-P410s traveltimes.
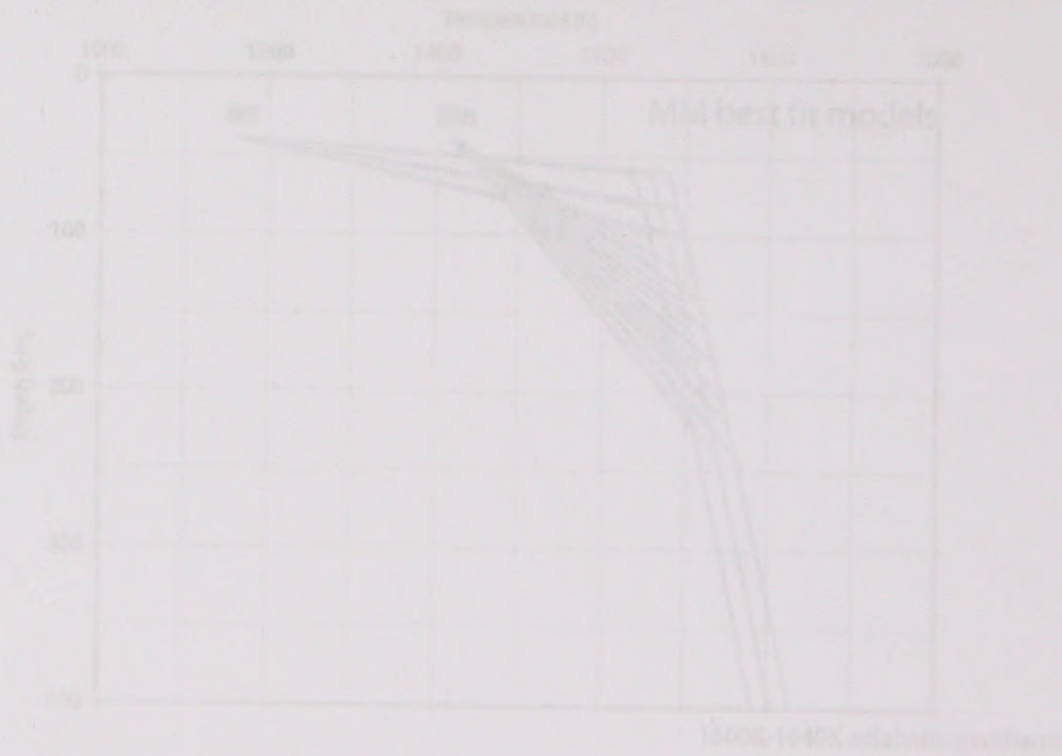
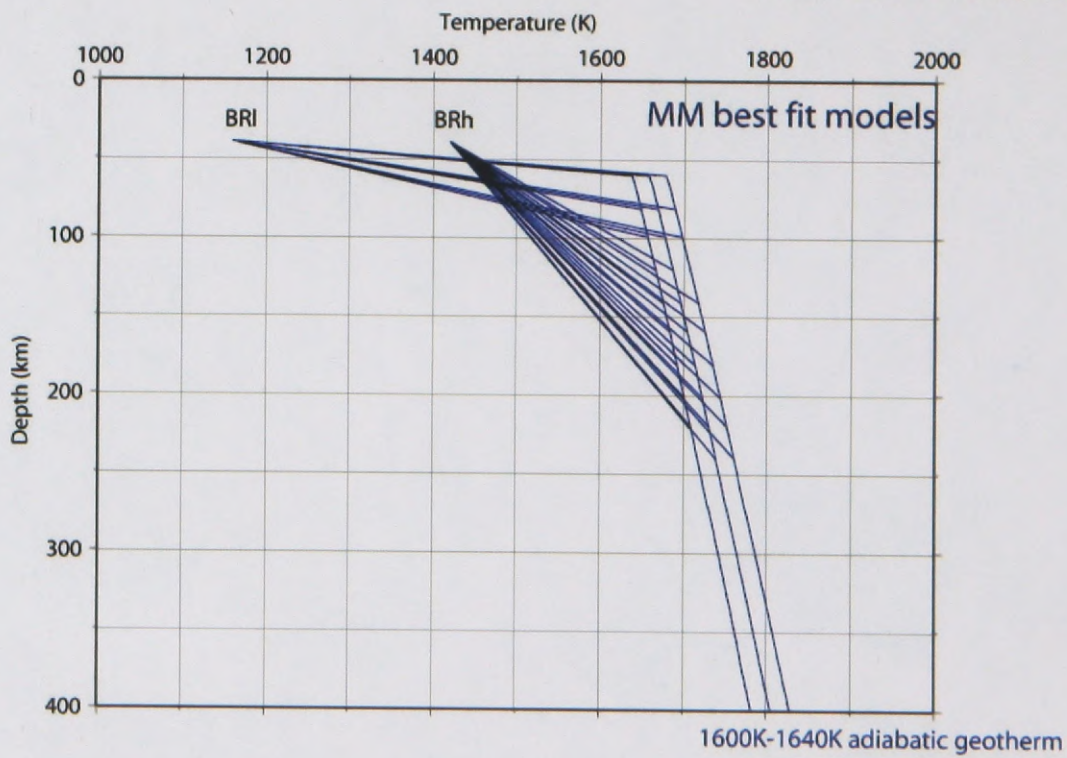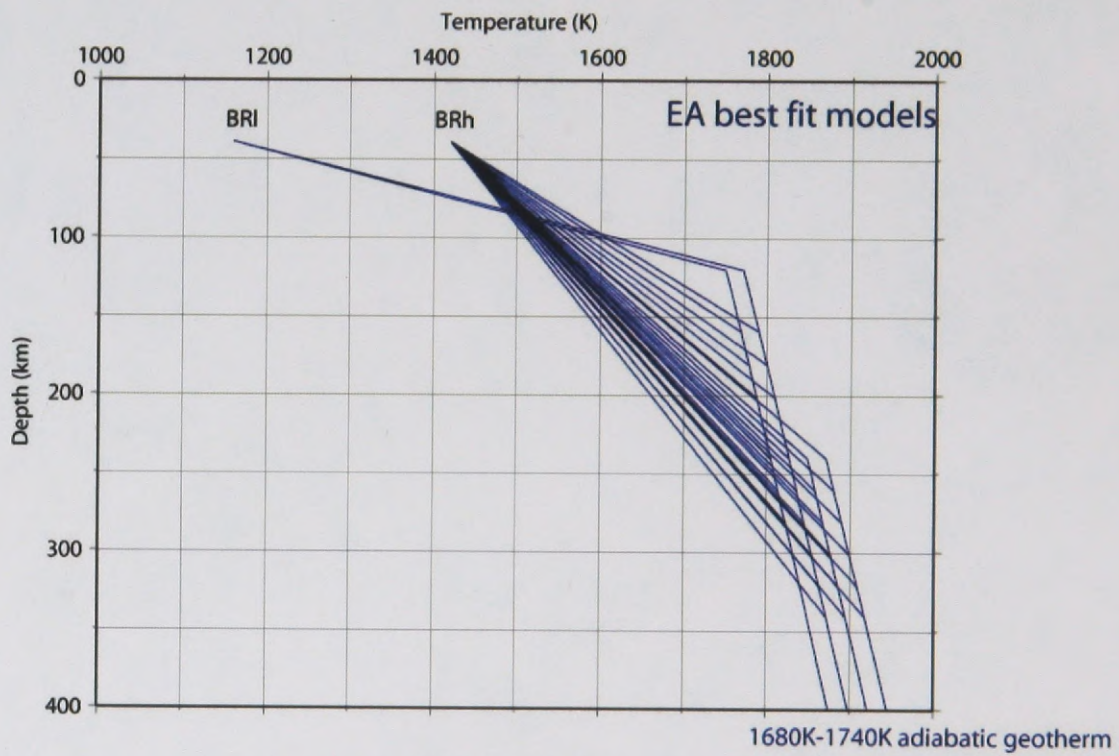Figure 18. Temperature profiles for the best fitting (top) EA and (bottom) MM shear velocity profiles of Figure 17.